Marine Mammal Science

MARINE MAMMAL SCIENCE, 32(3): 1044–1071 (July 2016)

DOI: 10.1111/mms.12323

Use of time-at-temperature data to describe dive behavior in five species of sympatric deep-diving toothed whales

Trevor W. Joyce,[1] Scripps Institution of Oceanography, University of California San Diego, 9500 Gilman Drive, La Jolla, California 92093, U.S.A.; **John W. Durban and Holly Fearnbach,** Southwest Fisheries Science Center, National Marine Fisheries Service, National Oceanographic and Atmospheric Administration, 8901 La Jolla Shores Drive, La Jolla, California 92037, U.S.A.; **Diane Claridge,** Bahamas Marine Mammal Research Organization, PO Box AB-20714, Marsh Harbour, Abaco, Bahamas; **Lisa T. Ballance,** Southwest Fisheries Science Center, National Marine Fisheries Service, National Oceanographic and Atmospheric Administration, 8901 La Jolla Shores Drive, La Jolla, California 92037, U.S.A. and Scripps Institution of Oceanography, University of California San Diego, 9500 Gilman Drive, La Jolla, California 92093, U.S.A.

Abstract

This paper develops and validates a method of using time-at-temperature (TAT) histograms from satellite transmitter tags to describe the dive activity patterns and approximate depth distributions of five deep-diving toothed whale species in the northern Bahamas. TAT histograms represent a bandwidth-conserving method of recovering a long-term proxy record of dive activity. However, using temperature to interpret TAT on a scale of approximate depths required the complex estimation of TAT histogram bin boundary depths in a dynamic oceanographic region. Here we evaluated the relative performance of four interpolation methods and a global reanalysis data assimilation model in estimating climatological isotherm depth surfaces within our study area. TAT-derived approximate time-at-depth (TAD) distributions aligned closely with directly observed TAD distributions from a smaller sample of depth-recording satellite tags deployed on separate individuals of each species. TAT-derived approximate depth distributions were also consistent with various published accounts for this suite of species. Estimating dive ranges and time budgets are important components of (1) understanding habitat overlap between species, (2) evaluating the potential role of these predators in meso- and bathypelagic ecosystems, and (3) assessing vulnerability and exposure to anthropogenic impacts.

Key words: dive behavior, spatial models, Odontoceti, Bahamas.

Deep-diving toothed whales (Suborder: Odontoceti) elicit considerable interest due to their exceptional diving capacity and potential ecological importance as apex predators in meso- and bathypelagic ecosystems (Noren and Williams 2000, Tyack *et al.* 2006, Lavery *et al.* 2010). Direct examination of the diverse niches occupied by different species in the deep-diving toothed whale foraging guild have been hampered to date by difficulties in directly observing their foraging activities at

[1]Corresponding author (e-mail: twjoyce@ucsd.edu).

depths (Macleod *et al.* 2003, Tyack *et al.* 2006, Hazen *et al.* 2011, Aoki *et al.* 2015). With minimal direct observations, vertical profiles of time spent at different depth and/or temperature strata in the water column can provide useful information to deduce differences in dive strategy and habitat use between species and sexes, as well as over diurnal cycles (Johnson *et al.* 2009). Moreover, deep-diving toothed whales in many regions are exposed to a range of potentially deleterious anthropogenic activities (Frantzis 1998, Laist *et al.* 2001, Cox *et al.* 2006, D'Amico *et al.* 2009). Thus, vertical distributions of time spent in the water column can also help monitor the relative exposures and responses of different species to anthropogenic threats.

Archival biologging instruments developed over the last 15 yr have considerably improved the understanding of the niche-spaces occupied by a growing number of deep-diving odontocete species. In particular, time-depth recording tags (TDR, *e.g.*, Hooker and Baird 1999), and digital acoustic recording tags (DTAG, *e.g.*, Johnson and Tyack 2003) have contributed to detailed descriptions of time spent at different depths in the water column. DTAGs also allow descriptions of habitat use, including the localization of search effort and prey capture attempts (Madsen *et al.* 2002, Miller *et al.* 2004*a*, Tyack *et al.* 2006, Watwood *et al.* 2006, Aguilar de Soto *et al.* 2008, Teloni *et al.* 2008). However, the close proximity necessary for deployment, and the lengthy follows necessary for the recovery of these platforms require extensive investment and labor input, which ultimately limits sample sizes. Moreover the noninvasive attachment and high-sampling frequency of these technologies limit their deployment duration to short time windows (typically <24 h), constraining analyses of lower-frequency variations in behavioral patterns such as shifts over diurnal or lunar cycles. Here we explore the complementary use of a satellite-linked telemetry platform that can provide relatively long and continuous, though indirect, proxy records of dive patterns and approximate depth ranges.

Smart Position Only Tags (SPOT; Wildlife Computers, Inc., Redmond, WA) and more recently developed depth-recording satellite transmitter tags (SPLASH; Wildlife Computers, Inc.), both provide satellite telemetry estimates of animal position through time using the Argos-satellite system (http://www.Argos-system.org). These small tags (49 g and 63 g, respectively) have become particularly useful for studies of cetaceans when implemented in the Limited Impact Minimally Percutaneous External Electronic Transmitter configuration (LIMPET; Andrews *et al.* 2008), because they can be reliably projected onto the dorsal fins of cetaceans from distances up to 25 m, greatly increasing the range of species that can be monitored using telemetry (Baird *et al.* 2011, Schorr *et al.* 2010, Durban and Pitman 2012). In addition to returning position information, SPOT tags can also be programmed to transmit highly compressed periodic records of the proportion of time that diving animals spend in different user-defined temperature strata within the water column. These summaries, in the form of time-at-temperature (TAT) frequency histograms, can be interpreted directly in terms of the thermoregulatory costs imposed by exposure to different water temperatures. However, in regions where the gradient of water-temperature with depth has been measured and is temporally relatively consistent, TAT summaries can also be used as proxies for time-at-depth, providing a useful source of information on diving behavior and time budgets.

In this study we developed and validated an approach for using TAT summaries to describe and compare the diving activity of five odontocete species within the Great Bahama Canyon, in the northern Bahamas. Considerable research interest has been focused in this region in response to a mass stranding event of beaked whales in

2000, coincident with naval sonar exercises (Balcomb and Claridge 2001, Cox *et al.* 2006). Subsequent research has also shown behavioral responses to sonar exposure among Blainville's beaked whales (*Mesoplodon densirostris*) on the U.S. Navy's Atlantic Test and Evaluation Center (AUTEC) range within this canyon system (McCarthy *et al.* 2011, Tyack *et al.* 2011, Moretti *et al.* 2014). A number of other species of deep-diving whales regularly occur in this region and are also potentially exposed to sonar sources, highlighting the need to fill key gaps in our understanding of their behavioral ecology in order to manage their vulnerabilities.

Here, we compare several approaches for empirically describing isotherm depths that separate TAT histogram categories across our study region and use temperature as a proxy to describe the proportion of time animals spend in different estimated depth strata. Subsequently, we validate these approximate depth distributions by comparing the estimated vertical habitat use patterns based on TAT with directly observed depth distributions from a small sample of SPLASH model LIMPET tags. These SPLASH tags were deployed in parallel with SPOT tag deployments in the later years of the study on the same suite of species in the same habitats. Due to their lighter weight, lower battery consumption, and limited transmission bandwidth requirements, SPOT tags typically provided longer and more continuous records of dive activity than SPLASH tags in this study. TAT-derived approximate depth distributions thus complemented the direct descriptions of dive behavior from SPLASH tags. The development and validation of this method allowed us to use a substantial legacy data set from SPOT tags that had accrued before SPLASH models became commercially available, and thus to more fully use all available data to fill key information gaps for deep-diving cetaceans in this strategically important region.

Methods

Study Area

This study was conducted in the Great Bahama Canyon region of the Bahamas archipelago in the western North Atlantic Ocean, between 23°N–27°N and 76°W–79°W. Tagging of five odontocete species was carried out in the deep-water channels of the NE and NW Providence Channels and Tongue of the Ocean (Fig. 1). Importantly for the estimation of isotherm depths, this study area is embedded within the western boundary current system of the North Atlantic Subtropical Gyre (Hamilton *et al.* 2005), which is an important consideration for estimating isotherm depths. It is situated between the Antilles Current (Lee *et al.* 1996, Olson *et al.* 1984) flowing along the eastern slope of the Bahamas archipelago, and the Florida Current flowing through the Florida Strait to the west of the study area (Hamilton *et al.* 2005, Wang and Mooers 1997). The northeast and northwest Providence Channels are open to both of these currents, although constricted by a shallow sill (664 m) near the western end of the NW Providence Channel. Thus, a temporally variable volume transport of 0.9–1.3 Sv (10^6 m^3/s) has been estimated to flow from east to west through this channel (Wang and Mooers 1997, Hamilton *et al.* 2005, Beal *et al.* 2008). Below ~800 m, along the eastern slope of Little Bahama Bank at 26.5°N, a deep western boundary current with a highly variable net southward flow has been measured from the shelf slope out to the eastern edge of the study area (Johns *et al.* 2008).

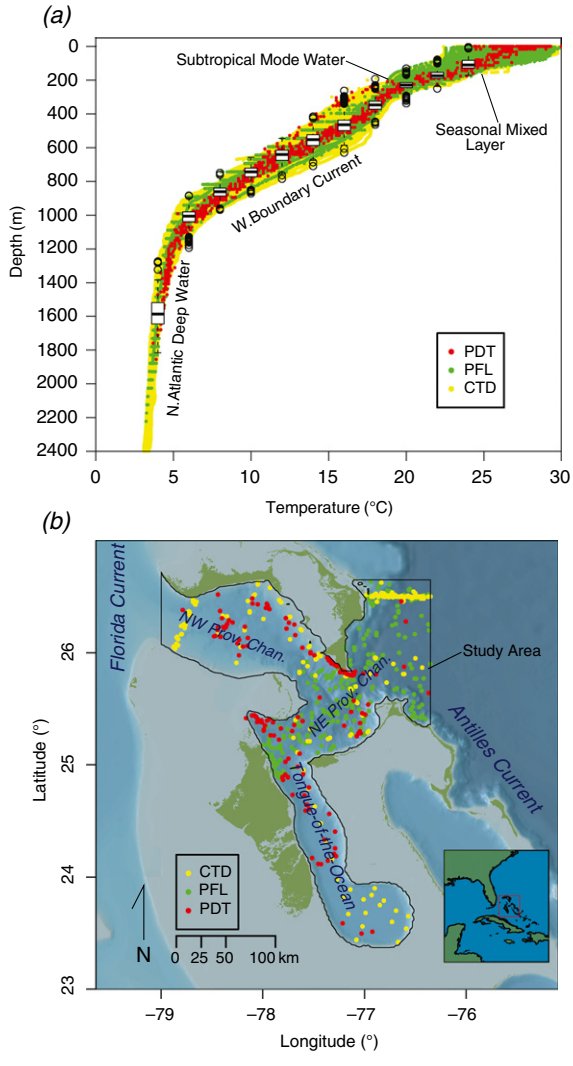

Figure 1. (a) Plot of temperature as a function of depth across all types of profiles within the study area. Temperature profile types included coarse-resolution profiles of depth and temperature (PDT, 2011–2014) recovered from SPLASH tag deployments on four species of cetaceans, as well as moderate- to high-resolution sampling from neutrally buoyant Argo profiling floats (PFL, 2004–2013) and conductivity temperature depth instruments (CTD, 1990–2013) from the World Ocean Database (WOD). Modified box plots have been overlaid on these profiles showing the central tendency (median) and depth variation of the even numbered isotherms between 4°C and 24°C. (b) Map showing sampling locations of these three types of temperature profile data that were employed in statistical descriptions of thermal structure in the NW Bahamas. The study area boundary and major geographic and oceanographic features are also labeled. The line features used to calculate the distance proxies across the Providence Channels (d_{chan}) and distance from the Florida Strait (d_{flst}) are highlighted in bold.

Study Species and Tagging

The telemetry data used in this analysis were collected over a 5 yr period (2009–2014) and comprised deployments of SPOT and SPLASH Argos satellite transmitters on five species of odontocetes: melon-headed whale (*Peponocephala electra*), short-finned pilot whale (*Globicephala macrorhynchus*), sperm whale (*Physeter macrocephalus*), Cuvier's beaked whale (*Ziphius cavirostris*), and Blainville's beaked whale (*Mesoplodon densirostris*). Whales were located using visual search effort with a mixture of line transect and *ad hoc* survey techniques from platforms ranging from small boats to large research ships, accompanied by passive acoustic monitoring using either a towed hydrophone array (Gillespie *et al.* 2009) or a fixed array on the AUTEC range (McCarthy *et al.* 2011). Two models of LIMPET satellite transmitting tags were used: SPOT (AM-S240A-C, Wildlife Computers Inc.; *e.g.*, Andrews *et al.* 2008) and SPLASH (Mk-10, Wildlife Computers Inc.; *e.g.*, Schorr *et al.* 2014). These tags were attached on or near the dorsal fins of free-ranging cetaceans using two minimally invasive 4.5–6.5 cm surgical grade titanium darts that were projected using a crossbow bolt from distances of 5–25 m. During intervals when these animals surfaced to breathe and exposed their dorsal fins above the surface, the tags transmitted a series of messages to overhead Argos satellites (http://www.Argos-system.org), which allowed the calculation of location estimates with associated error ellipse estimates. These messages also delivered a limited quantity of dive behavior data collected and summarized internally within the tag.

Dive information transmitted by SPOT tags was derived from a thermistor, whereas SPLASH tags combined pressure sensor and thermistor measurements. SPOT tag models transmitted a condensed summary of temperature readings collected at 10 s intervals, typically over a 6 h period (29/36 tags returned partial 1–5 h summaries at the beginning of deployments). SPOT temperature summaries were transmitted in the bandwidth-conserving format of TAT histograms, in which the proportion of time spent within 12 user-defined temperature categories (<4°C, 4°C–6°C, 6°C–8°C, 8°C–10°C, 10°C–12°C, 12°C–14°C, 14°C–16°C, 16°C–18°C, 18°C–20°C, 20°C–22°C, 22°C–24°C, and ≥24°C) was represented as a percentage of all observations within the sampling period. We compared TAT data sets from each species with small samples (see below) of dive depth observations from more expensive (1.64× cost) SPLASH tags. As permitted by Argos bandwidth, these SPLASH tags uploaded time series of depth observations with a sampling interval of 2.5 min. In addition to dive data, SPLASH tags occasionally transmitted coarse resolution profiles of depth and temperature (PDT), each containing minimum and maximum temperature observations over a 12 h sampling period on eight depth levels evenly spaced over the dive range of each specific tagged animal. The midpoints between minimum and maximum PDT temperature readings on each depth level were employed in conjunction with hydrographic survey data in estimating the depths of isotherms defining the boundaries of TAT histogram categories (see Isotherm Depth Estimation).

Location Estimation

Estimating the movements of tagged cetaceans through space proved to be an important initial step both in incorporating PDT data into spatial models of isotherm depths, and in predicting isotherm boundaries at the mean locations of TAT histograms. To estimate the maximum likelihood path of each tracked individual

through space, while accounting for Argos location estimates of varying precision, we used the R package *crawl* (Johnson 2013) to fit a Continuous Time Correlated Random Walk (CTCRW, Johnson *et al.* 2008) assuming the estimated error radii represented the standard deviations of normally distributed errors about each location (*e.g.*, Ford *et al.* 2013). Following initial model fitting, the measurement error shock diagnostic of de Jong and Penzer (1998) was used to eliminate significant outliers ($P \leq 0.01$), and the model was refitted to estimate a movement track for each whale. Tags for this study were scheduled to transmit up to 700 times during 12–18 h of each day, timed to coincide with passes of satellites from the Argos satellite system. Location estimates from the Argos system were therefore irregularly spaced, and we used a second run of CTCRW to predict locations at regular hourly increments over the duration of the track. The mean location of tags over TAT (6 h) and PDT (12 h) summary periods were calculated by averaging these hourly maximum likelihood CTCRW location predictions over the respective summary periods (Fig. 1, 2).

Isotherm Depth Analysis

To interpret TAT summaries of cetacean dive behavior on a biologically meaningful and intercomparable depth scale, we applied a range methods to estimate the climatological (*i.e.*, long-term mean) isotherm depth that defines the temperature boundaries of TAT histogram categories. Furthermore, to simultaneously account for spatial and temporal components of isotherm depth variability, we compared these climatological estimates based on direct observations with time- and location-specific potential temperature outputs from the Hybrid Coordinate Ocean Model (HYCOM) 1/12° global reanalysis. This reanalysis employed Navy Coupled Ocean Data Assimilation and an ocean generalized circulation model to produce daily estimates of ocean state variables (*e.g.*, potential temperature, potential salinity) at 40 standard depth levels over the period 1992 to 2014 (Chassignet *et al*. 2007). The observational data used in estimating isotherm depths included coarse depth-resolution PDT profiles from SPLASH tags. In addition, moderate to high vertical-resolution, quality-controlled hydrographic profile data from vessel-based conductivity-temperature-depth instruments (CTD), and drifting neutrally buoyant profiling floats (PFL) extracted from the World Ocean Database (WOD) online repository on 7 July 2014 (http://www.nodc.noaa.gov/OC5/SELECT/dbsearch/dbsearch.html) were also used in estimating isotherm depths. Although extensive CTD sampling dating to 1968 was available within the study area, we avoided sampling conducted prior to the advent of civilian GPS technology (~1990) because of the insufficient precision of CTD locations based on pre-GPS navigation tools.

A two-step process was applied in estimating the climatological depths of the relevant isotherms (4°C–24°C in 2°C increments). First the depth of each isotherm was estimated in the vertical z-dimension within each profile using a linear approximation between the temperature/depth observations bracketing the ith isotherm. An identical procedure was applied in each cell of HYCOM reanalysis (GLBu0.08) raster outputs to estimate the depth of the ith isotherm from 40 standard depth levels of potential temperature predictions (0 m, 2 m, 4 m, 6 m, 8 m, 10 m, 12 m, 15 m, 20 m, 25 m, 30 m, 35 m, 40 m, 45 m, 50 m, 60 m, 70 m, 80 m, 90 m, 100 m, 125 m, 150 m, 200 m, 250 m, 300 m, 350 m, 400 m, 500 m, 600 m, 700 m, 800 m, 900 m, 1,000 m, 1,250 m, 1,500 m, 2,000 m, 2,500 m, 3,000 m,

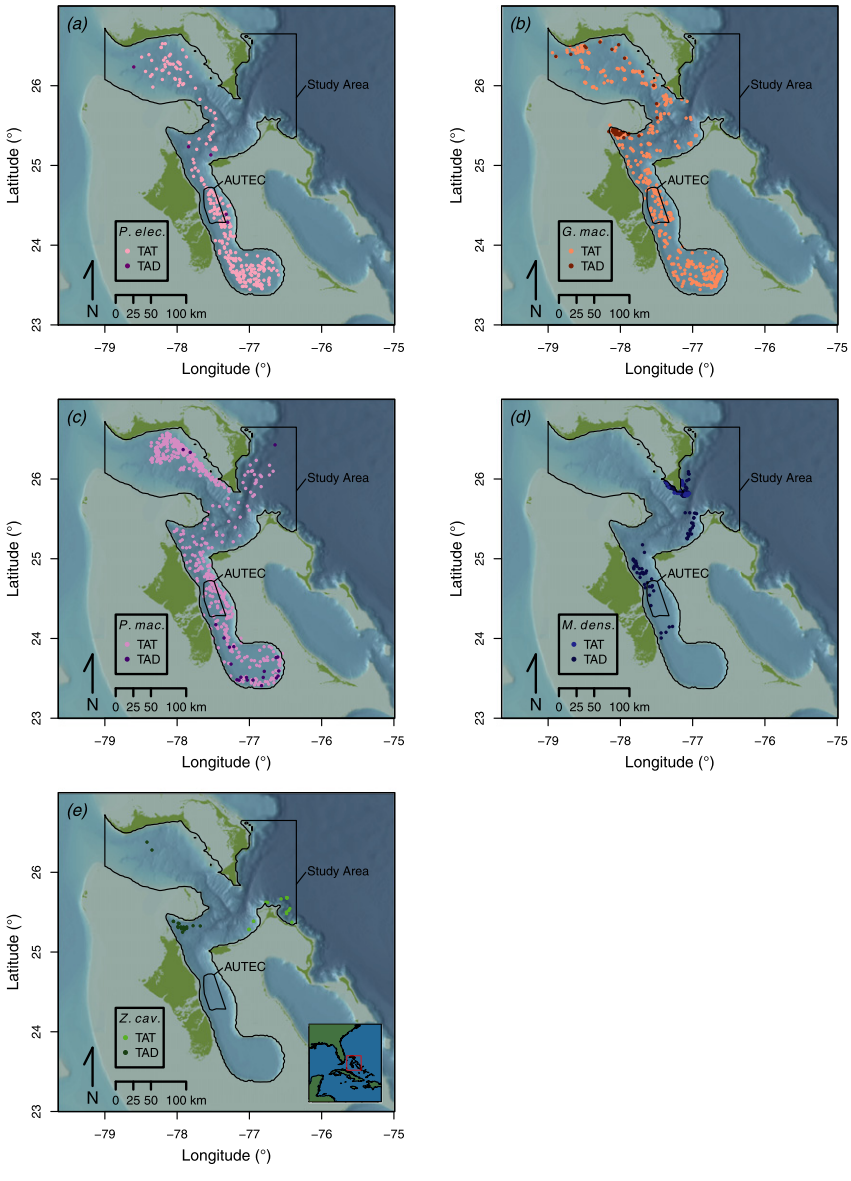

Figure 2. Mean locations of time-at-temperature (TAT) histograms and time-at-depth (TAD) histograms from transmitter tags deployed on each of five species in the Great Bahama Canyon: (a) melon-headed whale (*Peponocephala electra*, N_{SPOT} = 9 , N_{SPLASH} = 4), (b) short-finned pilot whale (*Globicephala macrorhynchus*, N_{SPOT} = 12, N_{SPLASH} = 3), (c) sperm whales (*Physeter macrocephalus*, N_{SPOT}=21, N_{SPLASH} = 6), (d) Blainville's beaked whale (*Mesoplodon densirostris*, N_{SPOT} = 3, N_{SPLASH} = 9), and (e) Cuvier's beaked whale (*Ziphius cavirostris*, N_{SPOT} = 1, N_{SPLASH} = 6). The mean locations were derived by fitting a movement model (Johnson *et al*. 2008) to smooth and filter irregularly spaced Argos telemetry estimates from SPOT and SPLASH tags, respectively. The study area boundary and U.S. Navy's Atlantic Test and Evaluation Center (AUTEC) are also shown.

4,000 m, and 5,000 m). Using the observational data, the *i*th isotherm was subsequently interpolated in *x*- and *y*-dimensions over the study area using (1) an overall mean depth, (2) grid cell mean depths at 0.1°, 0.5°, and 1.0° latitude and longitude resolutions, and (3) spatial models of isotherm depth. This two-step approach reduced the dimensions and complexity of isotherm depth interpolation and limited the degrees of freedom needed to fit isotherm depth models relative to a three-dimensional model of thermal structure. However, in low-resolution PDT profiles which contained only eight temperature-depth observations per profile, linear approximation between widely spaced data points introduced artifacts where the slope of the thermocline abruptly changed (see Fig. 2) (*e.g.*, such as at the 18°C–20°C subtropical mode water thermostad and at the 6°C base of the thermocline). To reduce this potential source of bias, PDT observations were excluded from spatial interpolations of the 20°C and 6°C isotherms, but were maintained in the remaining isotherm interpolations where they supplemented CTD and PFL sampling coverage within the otherwise sparsely sampled NW Providence Channel and Tongue of the Ocean (Fig. 2).

The goal of implementing interpolation methods more complex than a single overall mean isotherm depth (calculated using all available observational data in the study area) was to improve the precision of isotherm depth predictions by accounting for the spatial and/or temporal processes affecting the climatological isotherm depth. However, to account for the spatial component of the isotherm depth field variability, we first applied a grid-averaging approach, in which point observations were organized into grids covering the study area with cell dimensions of 1.0°, 0.5°, and 0.1° of latitude and longitude. Where present, the mean of all observations was calculated in each grid cell.

Using the linearly approximated depth of the *i*th isotherm (z_i) within each profile as a response variable, we fitted initial quadratic linear (LM) and generalized additive models (GAM) including five covariates, as well as interactions between each pair of covariates (Trossman *et al.* 2011). We used latitude (y), longitude (x), and Julian date (t, *i.e.*, numerical day within year) as initial covariates to explicitly model the spatial and seasonal components of variability in climatological z_i. We also evaluated the use of several proxy covariates to improve the representation of narrow topography-following features in LM and GAM based on the example of Roemmich and Gilson (2009). These covariates included distance-across-the-Providence-Channel (d_{chan}) and distance-from-the-Florida-Straight (d_{flst}) in the upper water column (>24°C–10°C). Distance-across-the-Providence-Channel (d_{chan}) provided a proxy for a gradient of isotherm depths within the thermocline (10°C–18°C) across the NE and NW Providence Channels resulting from a mean geostrophic flow of 0.9–1.3 Sv between the Antilles Current and Gulf Stream (Wang and Mooers 1998, Hamilton *et al.* 2005, Beal *et al.* 2008). Distance-to-the-Florida-Strait (d_{flst}) was similarly introduced as a proxy representing a time-varying recirculation of the Florida Current in the NW Providence Channel. The proxy variables d_{chan} and d_{flst} were calculated as minimum geodesic distances from the 50 m isobath surrounding Little Bahama Bank (Fig. 1), and a line traversing the western mouth of the NW Providence Channel (79.25°W, 25.96°N to 79.20°W, 27.10°N; Fig. 1), respectively. These distances were calculated using the function *gdist* in the R library *Imap* (Wallace 2012) and a geographic coordinate system based on the World Geodetic Survey 1984 datum. Distance-across-the-Providence-Channel (d_{chan}) was capped at the maximum breadth of the NE and NW Providence Channels (84.3km). In modeling isotherms at depths of 10°C and colder, simplified initial specifications of GAMs did not include day-of-year

or either of the distance proxies due to insufficient degrees of freedom given the relatively small number of profiles reaching these isotherms.

The optimal specification of quadratic LM for each isotherm was selected on the basis of Akaike's Information Criterion (AIC) score through a stepwise forward and backward covariate selection process implemented in the function *StepAIC* from the R library *MASS* (Venables and Ripley 2002). GAMs of the *i*th isotherm depth were fitted using univariate cubic shrinkage splines with a maximum of 3 degrees of freedom (df) and bivariate thin-plate shrinkage splines with a maximum of 20 df in the R library *mgcv* (Wood 2006). Shrinkage splines permit the effective degrees of freedom assigned by the *gam* algorithm to any smooth term to be penalized to 0, allowing *mgcv* to select an additive combination of predictors that minimizes generalized cross validation scores without resorting to a stepwise forward/backward variable selection process (Wood 2006). After fitting the quadratic linear model, Objective Analysis (OA) was implemented to interpolate the residual spatial autocorrelation left over after accounting for model covariates (Thomson and Emery 2014). This approach applies a Gauss-Markov function (Roemmich 1983), with parameters of decorrelation length scales in x- and y-dimensions and a signal-to-noise ratio, to weight the influence of nearby points as a function of proximity to the interpolation location (McIntosh 1990, Trossman *et al.* 2011). Decorrelation length scales were set at 84.3 km, which corresponded to the maximum perpendicular width of the NE and NW Providence Channels and Tongue of the Ocean.

To compare the relative predictive performance of various interpolation methods, we applied a 10-fold cross-validation to the overall mean, grid cell means, spatial models of isotherm depth, and objective analysis interpolations. This allowed determination of which method provided the most accurate, general, and precise prediction of the *i*th isotherm depth as well as an estimate of the uncertainty at the specific location and time of each TAT histogram. Point observations of each isotherm were randomly sorted into ten subsets and subsequently an overall mean, grid means, LM, GAM, and OA models were fitted on the basis of nine out of ten subsets. Predicted isotherm depths from these models were then compared with observed isotherm depth in the remaining subset, and this process was repeated such that each subset was used once as test data and nine times as training data. We compared five interpolation methods based on their utility in reducing the mean squared cross-validation prediction error (MSPE_i) relative to the MSPE of an overall mean.

$$\mathrm{MSPE}_i = \frac{1}{n}\sum_{j=1}^{n}\left(\mathrm{Observed}_{i,j} - \mathrm{Predicted}_{i,j}\right)^2 \quad (1)$$

HYCOM-estimated isotherm depths were similarly compared to other interpolation methods based on MSPE scores. For individual TAT histograms, each representing a unique location and date combination, the depth of the *i*th isotherm was predicted by the interpolation/reanalysis method that best minimized MSPE_i , while the overall range of observed depths at a given isotherm within the study area was used as an estimate of the uncertainty. When comparing two or more TAT histograms spanning multiple locations and dates, the depth of the *i*th isotherm was estimated by calculating a median of 0.05° grid cell predictions from the best interpolation method specific to the *i*th isotherm over the study area.

Validation of TAT

Rescaling TAT histograms from temperature to approximate depth categories required validation. We compared the vertical distribution of dive activity inferred from TAT histograms with a small sample (see below) of time-at-depth (TAD) summaries using the directly observed depth-time-series data available from SPLASH tags deployed on each study species. TAD summaries were assembled from depth time series observations collected at 2.5 min intervals and were subsequently organized into 6 h blocks starting at 0100, 0700, 1300, or 2100 local time (identical to TAT start times). From each 6 h block, a 12-category TAD histogram was calculated with depth breaks drawn from median best interpolation model predictions over the study area. Uploading full depth time series from SPLASH tags over the Argos satellite network required significantly greater transmission bandwidth than was typically available during relatively short surface intervals, thus very few 6 h blocks contain a complete and continuous depth time series. To qualitatively compare the vertical distributions of dive activity for each species inferred from TAT histograms to the time series of TAD histograms, we generated vertically stacked horizontal box-plots. These plots generally consisted of all the TAD histograms for a given species where the time series contained at least 50% (≥72/144) of the possible observations per 6 h block. Because this 50% threshold excluded all but one TAD sample for *P. electra*, a lower threshold of 25% (≥36/144) of observations per time block was applied to this species only. In *P. electra* and *Z. cavirostris* the limited available TAD histogram data substantially over-represented daytime and nighttime sampling, respectively. To compare these samples of TAD histograms to TAT observations that roughly overlapped in time-of-day, we restricted both TAD and TAT used in the box-plot comparison for these species to only daytime and nighttime records, respectively.

TAT and TAD samples, each containing multiple histograms per species, were evaluated for dissimilarity in the distribution of time spent within different depth strata. This comparison used a nonparametric mixed-effects permutational multivariate analysis of variance (perMANOVA) implemented in the program PRIMER+ (Clarke 1993). Before applying the perMANOVA test, categories representing the proportion of time spent within different temperature/depth strata were transformed into independent vectors using a centered log-ratio transformation (Aitchison 1986) implemented in the R package *compositions* (van den Boogaart and Tolosana-Delgado 2008). With two exceptions (a female and a subadult male sperm whale), each individual animal carried only one type of instrument, thus individual variability was treated as a random effect variable nested within each tag type. We then tested whether a fixed effect of tag type (*e.g.*, approximate temperature-based *vs.* directly observed) resulted in different multivariate distributions of time-at-depth within each species.

Results

Sampling

Over a 5 yr period (2009–2014), SPOT model telemetry and temperature recording tags were deployed on 46 individuals of five species of odontocete cetaceans (Table 1), with data collected widely throughout the study area (Fig. 1). From 2011

to 2014, 28 SPLASH model telemetry, pressure, and temperature recording tags were deployed on individuals of the same five species (Table 1). SPOT tags were attached to multiple individuals within a group on 23 occasions for four species (*P. macrocephalus*, *G. macrorhynchus*, *P. electra*, and *M. densirostris).* Tracks of these individuals show highly correlated postdeployment movements suggesting at least short-term persistence of social groups in these species (maximum tag duration: 92 d). Assuming a degree of dive synchrony within social groups (Pirotta *et al.* 2012, Aoki *et al.* 2013), the number of completely independent samples of dive behavior was thus less than the total number of tags attached (Table 1). Mean transmission durations of SPOT tags varied between 8.2 d for *P. macrocephalus* and 23.7 d for *Z. cavirostris*. Over this deployment period a total of 1,539 TAT histogram summaries were recovered, representing 9,115 h of dive activity across all species. TAT samples were primarily recovered from *P. macrocephalus*, *G. macrorhynchus*, and *P. electra* because of a programmatic emphasis on deploying SPLASH rather than SPOT tags on both beaked whale species (Table 1). Due to transmission bandwidth constraints during short surface intervals, only 216 6 h TAD summaries that were at least 50% complete were recovered, representing 1,296 h (896 h of raw depth time series sampling) of dive activity across all species. Over the period 2011–2014, 158 PDT profiles were recovered from 20 SPLASH tags on the basis of 12 h of temperature and depth sampling per profile.

Querying WOD for hydrographic profile data within our study area on 7 July 2014 returned 920 CTD casts over the period 1990–2013 and 899 PFL profiles from 2004 through 2013. The majority of CTD casts in our study area derived from repeat hydrographic sampling of the 26.5°N transatlantic RAPID-MOCHA transect (Fig. 2, right; *e.g.*, Smeed *et al.* 2014) in the NE corner of our study area, as well as a transect traversing the western entrance of the NW Providence Channel, with a minority of these CTD casts detailing hydrography within the interior of deep-water channels interspersed between the Bahamas banks (Fig. 2, right). The majority of PFL profiles in our study area were derived from multiple Argo floats that were advected into the eastern entrance of the NE Providence Channel and penetrated as far as the northern Tongue of the Ocean (Fig. 2, right). In addition, the 146 PDT profiles recovered *via* Argos satellites helped in filling some important gaps in the spatial coverage of our study area particularly in NW Providence Channel and in Tongue of the Ocean.

Location Estimation

TAT and TAD histogram locations calculated as a mean of hourly CTCRW-predicted locations are shown in Figure 1. The mean locations of *G. macrorhynchus*, *P. electra*, and *P. macrocephalus* TAT and TAD histograms reveal expansive dispersal and movement across the study area both over shelf-slope and deep-basin habitats. In contrast, tracks from SPOT tags and the more numerous SPLASH tags deployed on *Z. cavirostris* and *M. densirostris* indicate concentrations of activity over the shelf-slope and suggest moderate and limited dispersal, respectively. Tagged cetaceans, with the exception of five *G. macrorhynchus* individuals from two social groups and one *P. macrocephalus* individual, remained in the study area over the duration of tag battery and/or attachment life, and activity outside the study area was excluded from comparisons of TAT distributions due to significantly divergent thermal structure of the water column outside of the study area.

Table 1. Summary of Argos satellite LIMPET tag deployments on five species of deep-diving odontocete cetaceans in the NW Bahamas. SPOT model tag deployments were conducted over the period 2009–2014, while SPLASH model tag deployments were conducted over the period 2011–2014. The number of groups signifies the number of independent encounters with groups of odontocetes in which one or more animals were tagged. The number of time-at-temperature (TAT) recovered represents the number of 6 h summary histograms successfully downloaded from SPOT tags, while the number of time-at-depth (TAD) recovered represents the number of 6 h periods in which ≥50% (≥25% for *P. electra*) of depth time series observations were downloaded from SPLASH tags.

Species	SPOT deployments	SPLASH deployments	Number of groups	TAT recovered	TAD recovered	Mean deployment duration (d, minimum-maximum)
Peponocephala electra	9	4	6	274	5	9.51 (0.02–38.79)
Globicephala macrorhynchus	12	3	6	612	53	15.67 (0.37–40.80)
Physeter macrocephalus	21	6	13	563	23	8.20 (0.01–17.76)
Mesoplodon densirostris	3	9	9	28	119	16.41 (0.01–45.64)
Ziphius cavirostris	1	6	6	24	20	23.72 (8.53–90.14)

Isotherm Depth Analysis

Simultaneously plotting all of the temperature profile data with respect to depth revealed that, with the exception of the seasonally variable mixed layer (23°C–29°C), the subtropical mode water (18°C) and the North Atlantic Deep Water (NADW, <4°C) temperatures declined nearly linearly as a function of depth between 150 and 1,200 m depth (Fig. 2a). This approximately linear decline of temperature over much of the vertical range used by the five species of deep-diving odontocetes provided considerable resolution to differentiate the depth ranges of TAT histograms bins. However, the overlay of boxplots at the relevant temperature boundaries between 4°C and 24°C on top of the aggregate profiles (Fig. 2a) illustrates the considerable variation in isotherm depth across the study area, ranging from 542.8 m (1,273.1–1,815.9 m) at the 4°C isotherm to <172.1 m (76.9–249.0 m) at the 22°C isotherm. At least part of this variation is related to consistent spatial and/or temporal processes. A portion of the variability in the depth of the 22°C and 24°C isotherms is attributable to seasonal variation in the depth of the mixed layer, which can extend as deep as 150 m and as cold as 23°C in winter (Fig. 2, left). Furthermore, the vertical spreading of profiles between the 18°C subtropical mode water thermostad and approximately 10°C reflects geostrophic flows between these isotherms (1) along the eastern slope of Great and Little Bahama Banks and (2) through the NE and NW Providence Channels (Fig. 2a).

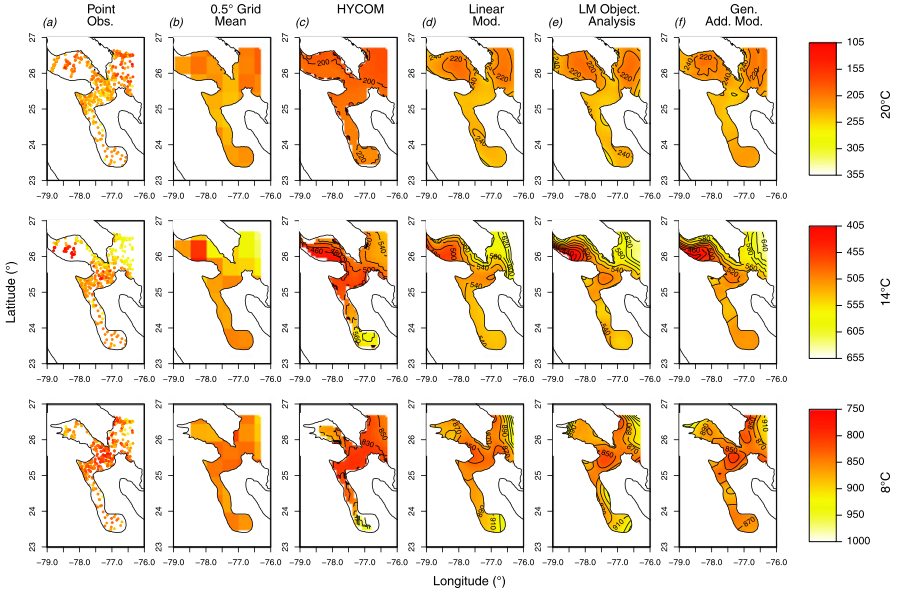

Figure 3. Prediction surfaces of the (a) linearly approximated depth observations and estimated mean depth field of three example isotherms (8°C, 14°C, and 20°C), that were predicted using five interpolation methods: (b) 0.5° grid cell mean, (c) HYCOM reanalysis, (d) quadratic linear model, (e) objective analysis based on the quadratic linear model, and (f) generalized additive model. The color scale in each panel represents a 250 m range centered on median observed depth of each displayed isotherm, thus the relatively muted color contrast in the 20°C series of plots reflects the lower total variability in isotherm depth at this temperature level when compared with the 8°C and 14°C series of plots.

The interpolation approach of taking the mean of observations within grid cells begins, at a coarse resolution, to address the spatial component of variability in climatological isotherm depth fields (Fig. 3b). Grid cell mean isotherm depths calculated at the 0.5° spatial resolution provided the greatest detail to resolve the spatial component of isotherm depth field variability (Fig. 3b), while still providing gapless coverage over almost all of the study area. This grid resolution revealed a deeper pool of warm water (14°C) in the western North Atlantic subtropical gyre to the east of the study area, as well as some indication of a temperature gradient along the eastern edge of the Bahamas banks and through the NW Providence Channel. The 0.1° resolution interpolation (not shown in Fig. 3) was more accurate than the 0.5° at the scale of individual TAT histograms. However, it was of limited utility as a general interpolation of the isotherm depth field due to numerous missing values in grid cells where observational data was not available. Conversely, the 1.0° grid resolution (also not shown) was too coarse to resolve gradients across the narrow interior channels between Bahamas banks.

Explicitly modeling the variation in isotherm depths using LM, GAM, and Objective Analysis improved the resolution of the climatological isotherm depth fields with respect to a single overall mean (Table 2), while simultaneously accounting for both spatial and temporal components of variability. Spatial and temporal covariates, including Julian date and the interaction of latitude and longitude, were selected as significant correlates explaining a portion of the variation in the depth field of the 20°C–24°C isotherms in both GAM and LM. Spatial covariates including the interaction of latitude and longitude, distance across the Providence Channels, and distance to the Florida Strait improved the prediction of 10°C–18°C isotherm depths in GAM and LM (Table 2). Below 10°C, the interaction of latitude and longitude proved to be the most important covariate in GAM fits. Spatial autocorrelation was indicated in the 10°C–18°C LM residuals and 14°C–16°C GAM residuals, thus Objective Analysis was implemented at these depths (Table 2). The comparison of isotherm depth predictions and HYCOM reanalysis climatology in Figure 3 shows a qualitative correspondence between the observed depths and the isotherm depth fields predicted by grid cell means, reanalysis outputs, and the various model based interpolation methods. This visual correspondence is confirmed by pairwise Pearson correlation coefficients between different prediction methods ranging, for example, from 0.80 to 0.88 in the 16°C isotherm (Table 3).

Table 2 presents a comparison of cross-validation and reanalysis prediction errors. It highlights the relative utility of various interpolation models and HYCOM reanalysis outputs in improving the prediction of isotherm depths at unobserved locations and times. In particular, the decrease in the MSPE using GAM, LM, and Objective Analysis depth predictions between 10°C and 18°C, reflects the utility of these models in accounting for the spatial structure of geostrophic currents at these depths. The climatological view of HYCOM outputs reveals the same general spatial patterns of isotherm depths as the other interpolation methods, which is corroborated by relatively high correlation coefficients shown in (Table 3). However, as indicated by the generally much larger MSPE values (Table 2), as well as the depth contours in Figure 3, the HYCOM outputs exhibited a systematic shallow bias with respect to the directly observed isotherm depths. The best models selected for each isotherm of interest on the basis of MSPE (Table 2) were quadratic LM between 22°C and 24°C, GAM at 20°C, and quadratic LM with objective analysis between 4°C and 18°C. These models were subsequently used to estimate depth

Table 2. Summary of depth and temperature (N_{PDT}) profiles from SPLASH tags, conductivity-temperature-depth (N_{CTD}) profiles, and neutrally buoyant profiling float (N_{PFL}) profiles used in isotherm depth analyses. Additionally, estimated isotherm depths, and cross-validation mean squared prediction errors (MSPE) for various interpolation methods are reported at the temperature boundaries of time-at-temperature histogram categories. Isotherm depths are reported as an overall mean depth (Depth overall), including the range of observed depths (Depth min., Depth max.), as well as the median of predicted depths (Depth best) within the study area from the best interpolation model for each temperature level. The best interpolation method for each isotherm (shown in bold) was selected on the basis of the lowest MSPE score from the overall mean, a 0.5° latitude × 0.5° longitude grid mean, linear model (LM), linear model with subsequent optimal interpolation (LM OA), generalized additive model (GAM), and HYCOM reanalysis.

Isotherm	*N* PDT	*N* CTD	*N* PFL	Depth overall	Depth min.	Depth max.	Depth best	MSPE overall	MSPE grid 0.5°	MSPE LM	MSPE LM OA	MSPE GAM	MSPE HYCOM
24	146	237	192	100.59	2.33	172.11	109.02	1,389	1,160	769	816	**766**	740
22	146	269	226	169.67	76.92	248.97	174.98	814	516	442	434	**429**	990
20	144	263	226	229	129.81	336.69	233.54	800	600	**485**	491	505	1,274
18	144	235	225	347.4	191.23	462.97	342.33	1,488	690	636	**571**	590	4,783
16	141	219	224	463.51	261.27	629.32	452.07	2,663	951	912	**657**	672	4,971
14	139	200	223	554.43	414.45	708.56	548.8	2,243	985	800	**572**	627	4,739
12	133	190	220	645.61	545.11	784.3	642.21	1,699	904	678	**587**	630	5,039
10	121	183	220	746.36	657.19	871.05	753.31	1,367	1,003	759	**709**	715	3,882
8	110	164	216	863.37	747.96	968.18	878.46	1,342	1,197	888	**833**	936	3,840
6	87	155	202	1,013.77	883.21	1,193.07	1,030.14	2,838	2,639	1,845	**1,742**	1,985	5,712
4	9	116	55	1,577.45	1,273.1	1,815.87	1,573.35	1,0150	9,789	**8,667**	9,101	9,153	28,020

Table 3. Pearson correlation coefficients (*r*) of isotherm depths predicted by each pair of interpolation or reanalysis methods at the temperature boundaries of time-at-temperature histogram categories.

Isotherm	Grid 0.5°: LM	Grid 0.5°: GAM	Grid 0.5°: LM OA	Grid 0.5°: HYCOM	LM : GAM	LM : LM OA	LM : HYCOM	GAM : LM OA	GAM : HYCOM	LM OA : HYCOM
24	0.29	0.25	0.28	0.34	0.53	0.79	0.78	0.08	0.88	0.76
22	0.79	0.83	0.77	0.66	0.92	0.87	0.61	0.91	0.71	0.66
20	0.69	0.80	0.72	0.35	0.81	0.89	0.41	0.82	0.29	0.40
18	0.85	0.88	0.82	0.01	0.89	0.85	0.19	0.95	0.11	0.19
16	0.83	0.85	0.82	0.32	0.88	0.86	0.45	0.98	0.45	0.50
14	0.78	0.80	0.74	0.23	0.89	0.89	0.43	0.96	0.37	0.48
12	0.75	0.84	0.76	0.10	0.84	0.91	0.37	0.91	0.22	0.39
10	0.63	0.74	0.65	0.16	0.79	0.85	0.48	0.84	0.24	0.43
8	0.52	0.62	0.56	0.31	0.58	0.60	0.53	0.76	0.28	0.46
6	0.31	0.42	0.30	0.08	0.29	0.63	0.03	0.71	0.11	0.03
4	0.25	0.77	0.24	0.14	0.17	0.92	0.05	0.10	0.04	0.08

Table 4. Results of mixed-effects permutational multivariate analysis of variance (perMANOVA) comparison of centered log-ratio transformed time-at-depth (TAD) and time-at-temperature (TAT) distributions within each species implemented in the program PRIMER+. After accounting for individual variability as a random effect variable nested within each tag type, none of these comparisons indicate a significant multivariate difference between summary types (*e.g.*, TAT and TAD).

Species	Variable	Effect type	df	*F*	*P*
Peponocephala electra	Individual	Random	9	2.8653	0.001
	Summary type	Fixed	1	0.4894	0.684
Globicephala macrorhynchus	Individual	Random	10	2.5533	0.001
	Summary type	Fixed	1	1.3464	0.311
Physeter macrocephalus	Individual	Random	19	5.5137	0.001
	Summary type	Fixed	1	0.8948	0.470
Mesoplodon densirostris	Individual	Random	5	3.5048	0.001
	Summary type	Fixed	1	0.9719	0.280
Ziphius cavirostris	Individual	Random	2	3.6920	0.002
	Summary type	Fixed	1	1.6730	0.188

and uncertainty of isotherm boundaries at TAT locations. Study-area-wide medians of isotherm depth fields predicted from these models at a 0.05° grid cell resolution were subsequently used in the depth scales shown in Figures 4 and 5. These median predicted isotherm depths (Fig. 4c, f) yielded very similar behavioral patterns to spatially varying estimates of isotherm depths (Fig. 4b, e), even when individuals ranged widely within the study area (Fig. 4d–f).

Validation and Interpretation of TAT

When qualitative comparisons are constrained to samples that overlapped in time of day, there is a close correspondence for each species between the approximate dive depth distributions inferred from TAT histograms (SPOT) with TAD histogram summaries from SPLASH tags (Fig. 5). Additionally, mixed effects per MANOVA results summarized in Table 4 indicate that distributions of time in different depth categories did not differ significantly on the basis of sampling method (*e.g.*, TAT *vs.* TAD), when individual variation was explicitly treated by including individual random effects.

Comparisons of depth ranges and patterns of time at depth using both methods reveal distinct species-specific modes of vertical habitat use (Fig. 5). However, because of the large imbalance of daytime to nighttime TAD profiles in *P. electra,* both TAT and TAD were restricted to daytime periods only in Figure 5. As a result, the distribution shown in Figure 5 poorly represents the overall pattern of dive activity in *P. electra* and the overall dive pattern for *P. electra* is more clearly shown in Figure 4a–c. The proportion of time that *P. electra* and *G. macrorhynchus* spent in sequential depth/temperature strata declined monotonically with increasing depth and lacked distinct deep activity peaks at the resolution of our analysis. Based on TAT data, the dive distributions of *P. electra* and *G. macrorhynchus* reached maxima of approximately 350–450 m (16°C–18°C) and 1,000–1,500 m (4°C–6°C), respectively. In both TAT and TAD, *P. macrocephalus* exhibited distinctly bimodal distributions of time at depth, with a broad peak of time spent between approximately 550–1,000 m (6°C–14°C), and a highly variable amount of time spent in the

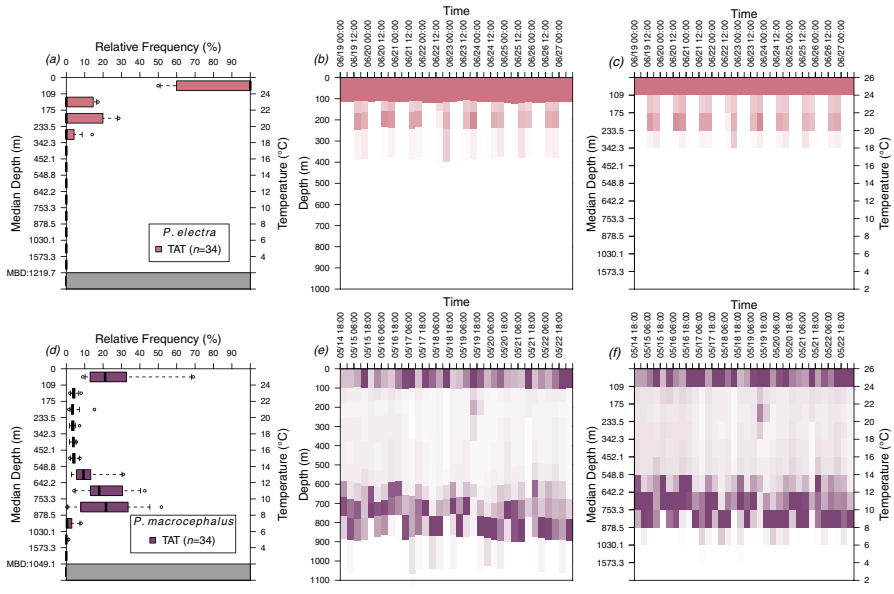

Figure 4. Illustrating three representations of 8.5 d time series of melon-headed whale (*Peponocephala electra*, (a–c), and sperm whale (*Physeter macrocephalus*, (d–f) time-at-temperature (TAT) histograms. Column 1 shows the median and variability in the proportion of time spent in 12 depth/temperature strata in a box-plot representation. Column 2 shows a time series representation with a fixed depth scale and variable box dimensions representing the local estimated depths of TAT strata. Column 3 shows the same data in an analogous representation, but with a depth scale that indicates the study-area-wide central tendency of isotherm depths and internal box dimensions that remain fixed.

uppermost depth and temperature strata ranging from <10%–100%. Both beaked whales, *Z. cavirostris* and *M. densirostris*, exhibited similarly bimodal distributions of time spent as a function of depth. *M. densirostris* displayed a deep peak of time spent between approximately 750 m and 1,500 m (4°C–10°C), while *Z. cavirostris* exhibited an analogous maximum, but slightly deeper between approximately 850 m and 1,500 m (4°C–8°C) in both TAT and TAD distributions. Finally, the discrepancies in the proportion of time spent in the upper two temperature-depth strata in *Ziphius* (Fig. 5) can be attributed to small sample sizes and individual differences in near-surface "bounce" dive depths.

Discussion

Validation of TAT

The comparison of approximate TAT-derived depth distributions from SPOT tags with directly observed TAD from SPLASH tags (Fig. 5) indicates that, despite markedly different sample sizes (Table 1) and sampling rates (10 s *vs.* 2.5 min), and even after accounting for interindividual variation in dive behavior, these two approaches converged on similar descriptions of dive behavior

patterns in our study species (Fig. 5, Table 4). Moreover, TAT-derived descriptions are also consistent with published accounts of diving activities, where available, for these species. Deep peaks of *P. macrocephalus* dive activity observed in both TAT and TAD (Fig. 5, ~550–1,000 m) were comparable to the peaks of time spent at depth by a similar demographic mixture of adult female and subadult males as those tagged in the Gulf of Mexico, western Atlantic Ocean, and Mediterranean Sea (Watwood *et al*. 2006). Animal-borne acoustic sensor data in Watwood *et al.* (2006) showed a peak of prey capture attempts, inferred from "buzz" vocalizations, at 700–800 m, which falls within the center of the TAT-derived approximate depth distribution. Similarly, the peaks of time spent by *Z. cavirostris* between ~850–1,500 m and by *M. densirostris* between ~750–1,500 m in TAT, closely overlapped the depth strata where maximum dive depths (*Z. cavirostris*: 1,450 m and *M. densirostris*: 890–1,408 m) were reported from TDR studies by Baird *et al.* (2006) in Hawaii. This peak also overlapped the mean maximum foraging dive depth in 11 of 14 *M. densirostris* dive records in the Canary Islands (Arranz *et al.* 2011). The approximate depth range of the deep activity peak estimated for *Z. cavirostris* in this study also overlapped the peak of echolocation buzzes recorded in a DTAG study of *Z. cavirostris* in the Ligurian Sea (Tyack *et al.* 2006). However, the diving range identified from TAT histograms in our study only overlapped the peak of benthic boundary layer buzzes and not the shallower open water mesopelagic peak of buzzes recorded in a DTAG study of *M. densirostris* in the Canary Islands (Arranz *et al.* 2011). Although the maximum dive depth of *Ziphius* reported in the Southern California Bight (2,992 m, Schorr *et al.* 2014) considerably exceeded the maximum recorded in our study (1,722 m), the mean deep dive duration and mean maximum dive depth in our SPLASH tag data were both consistent with the values reported by Schorr *et al.* (2014). Preliminary examination showed that *Z. cavirostris* dives ranged close to the benthos in the areas where tagged animals occurred within our study area, and thus the discrepancy between our deepest observation and Schorr *et al.* (2014) may relate to the capacity of this species to dive deeper when not constrained by the relatively shallow bottom depths found in much of our study area. Dive patterns of *G. macrorhynchus* in both TAT and TAD distributions reached a similar maximum depth strata (TAT: ~1,000–1,500 m, TAD: 840 m) to those reported by Aguilar de Soto *et al.* (2008; 1,019 m). Additionally, the gradual decline in time spent as a function of depth (Fig. 5), and the lack of a deep activity peak in this species, also reflected a similar dive pattern to the highly aerobic deep daytime foraging dives and relatively shallower nighttime foraging dives exhibited by *G. macrorhynchus* in the Canary Islands (Aguilar de Soto *et al.* 2008). To the best of our knowledge this is the first biologging effort to describe the distribution of subsurface activity in *P. electra*.

Interpretation of TAT

TAT histograms interpreted on a scale of approximate depths provided a relatively coarse but useful means of differentiating dive depth ranges and time budgets between species and sexes, particularly when interpreted in conjunction with complementary information from SPLASH tags and published high resolution DTAG and TDR data. For example these tools allowed the description of *P. electra* as a nearly exclusively nocturnal upper-mesopelagic diver (~150–400 m, Fig. 4). This pattern of

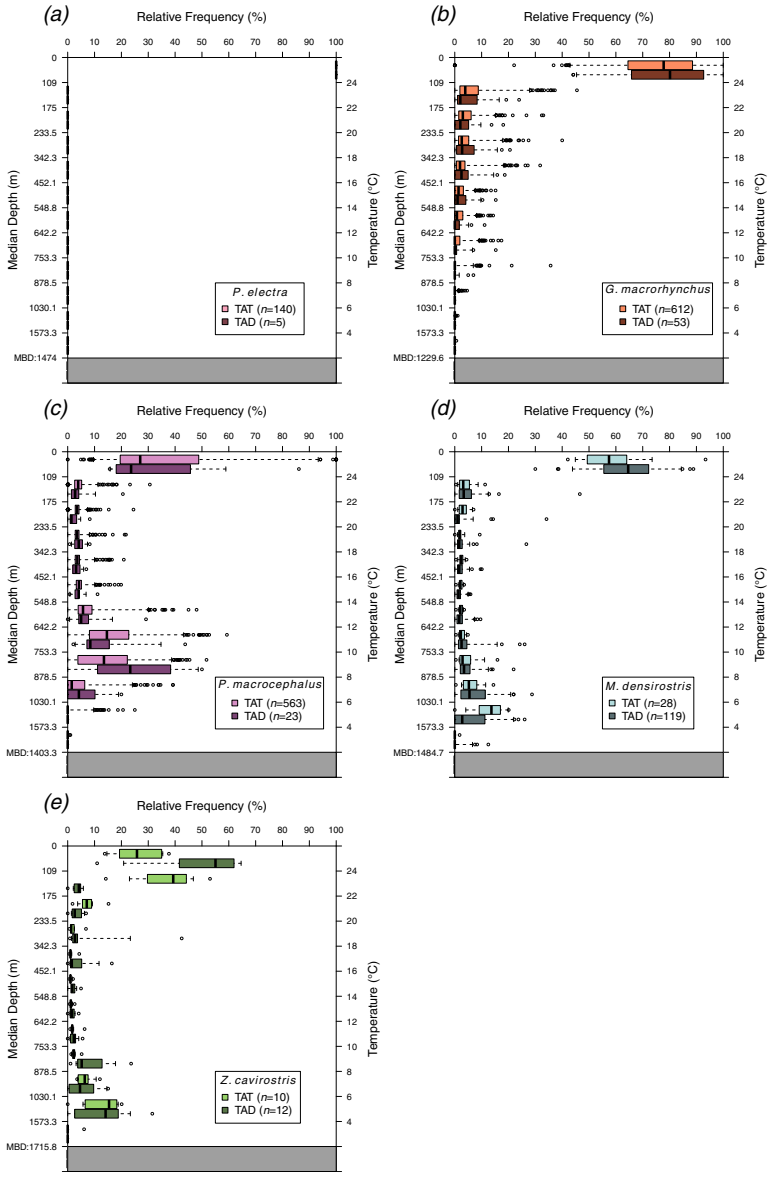

Figure 5. Boxplots comparing approximate dive depth distributions derived using time-at-temperature (TAT) data from SPOT satellite tags, to time-at-depth (TAD) summaries, generated from directly observed dive depth time series from SPLASH satellite tag deployments on (a) melon-headed whales (*Peponocephala electra*), (b) short-finned pilot whales (*Globicephala macrorhynchus*), (c) sperm whales (*Physeter macrocephalus*), (d) Blainville's beaked whales (*Mesoplodon densirostris*), and (e) Cuvier's beaked whales (*Ziphius cavirostris*). Mean of bottom depths (MBD) at the continuous time correlated random walk (CTCRW) maximum likelihood estimated locations of TAT histograms are shown on each plot.

habitat use showed elements of commonality with the dive behavior of its closest relative in our study *G. macrorhynchus*, which also dove more frequently during nighttime periods. However as shown by Aguilar de Soto *et al.* (2008), *G. macrorhynchus,* unlike *P. electra*, also dove during daytime periods though typically less frequently and to deeper lower-mesopelagic depths. The interpretation of TAT on a scale of approximate depths also allowed the confirmation of a broad differentiation within our study area between the central to lower mesopelagic peak of dive activity in *P. macrocephalus*, and the lower mesopelagic and upper bathypelagic dive activity peaks of *M. densirostris* and *Z. cavirostris* (Fig.5). Calculating the proportion of time that different species spent below species-specific foraging depth thresholds identified from DTAG acoustic, depth, and accelerometry data (Tyack *et al*. 2006, Watwood *et al*. 2006, Aguilar de Soto *et al.* 2008), further allowed comparisons of the minimum proportion of time that different species spent foraging. Time series of TAT histograms from SPOT tags also provided a useful complement to the typically shorter duration (due to higher battery consumption) and more discontinuous records of dive behavior produced by SPLASH tags in this study, allowing the identification and confirmation of diurnal and even lunar patterns of variation in vertical habitat use (Baird *et al*. 2008). That said, pressure recording SPLASH tags can be programmed to optimize satellite data acquisition by prioritizing data packages of different sizes ranging from full and summarized dive profiles to time-at-depth histograms. The relatively discontinuous depth time series records collected in this study thus reflected the prioritization of other data types at the expense of a continuous time series, rather than an innate limitation of the SPLASH tag. Finally, the larger sample sizes afforded by incorporating legacy SPOT data with SPLASH tag data allowed wider perspectives on intrapopulation variation and particularly, on intersexual differences in dive behaviors, and thus allowed a more full use of all available data to fill key information gaps for these deep-diving cetaceans.

Limitations of Thermal Proxy For Depth

Because of the dynamic nature of oceanic temperature fields in space and time, using temperature as a proxy for depth presented a range of limitations and required a number of estimation assumptions. Deriving model estimates of climatological isotherm depth fields and of the uncertainty surrounding these depth surfaces, particularly in a hydrodynamically complex region such as our study area, first required (1) a robust oceanographic data set, (2) an assumption of residual normality, and (3) persistent spatial- and/or temporal-variability in the climatological mean state that could be effectively modeled as a function of random variables (*e.g.*, x, y, d_{flst}, d_{chan}, t). In the first estimation requirement, our study benefited from temperature profile data from the animal-borne sensors on SPLASH tags, as well as a relatively dense program of hydrographic sampling in our study area, due primarily to an interest in quantifying the Atlantic Meridional Overturning Circulation (AMOC) transport (Wang and Mooers 1997, Hamilton *et al.* 2005, Beal *et al.* 2008, Kanzow *et al.* 2010). The second assumption of approximate residual normality was evaluated and supported in the model validation step through the examination of Q-Q plots. The third assumption, about persistent spatial processes and structures, was supported by the relatively low variability of flow through the NW Providence Channel reported by Hamilton *et al.* (2005), as well as the reduction in MSPE and model residual standard deviation achieved by LM and GAM interpolations, particularly between 10°C and 18°C (Table 2). Seasonal variation in the

vertical mixing affecting the depths of the 22°C and 24°C isotherms, as well as a small seasonal cycle in AMOC (Kanzow *et al.* 2010), were similarly captured by the inclusion of day-of-year (t). This is reflected in a reduction in MSPE of both LM and GAM interpolations with respect to an overall mean encompassing all depth observations at these isotherms. The descriptions of isotherm depth achieved in this study were also consistent with the isotherm and isopycnal structures identified along transects across the NW Providence Channel that were used in estimates of volume transport from the NW Providence Channel into the Florida Current (Leaman *et al.* 1995, Wang and Mooers 1998, Hamilton *et al.* 2005, Beal *et al.* 2008).

Both the use of temperature as a proxy for depth and the vertical and temporal binning inherent in TAT summaries limited the interpretation of finer resolution dive behavior in several important respects. To simultaneously interpret multiple TAT histograms in terms of approximate time-at-depth distributions, we primarily report isotherm depths using climatological estimates derived from optimal model interpolations that incorporated all the available hydrographic sampling over the last 24 yr (1990–2014). However, the instantaneous isotherm depths at any given TAT location and time may have differed from these climatological isotherm depth surfaces, although they are likely contained within the overall ranges of observed values at each isotherm (Fig. 2). This divergence of the instantaneous values from the climatological state is indicated by the spread of model residuals and cross-validation prediction errors after accounting for spatial and seasonal processes. Specifically, we considered daily HYCOM reanalysis outputs to simultaneously account for the spatial and temporal components of isotherm depth variability. However, the global HYCOM data assimilation model outputs performed relatively poorly as predictors of the observed temperature-depth data (Table 2) and also exhibited a systematic shallow bias. Thus, the HYCOM reanalysis was not used to interpret TAT histograms (Table 2), and the use of climatological estimates required us to refer to time-at-depth distributions inferred from TAT histograms as *approximate* depth distributions throughout this paper (Fig. 4, 5). Defining the approximate depth axis of box-plots (Fig. 4, 5) that compared multiple TAT histograms across different locations and times further necessitated the use of median-predicted isotherm depths over the entire study area or a subregion of interest, as opposed to a location- and time-specific estimate of climatological isotherm depths specific to any single TAT histogram. As an alternative to defining a single vector of overall median climatological isotherm depth estimates along this axis, we developed an alternative graphical representation. Multiple TAT histograms are shown as time-series where the depth axis is fixed and colored boxes represent the proportion of time spent in particular temperature/depth strata. These vary in vertical dimension in response to model-predicted local climatological isotherm depths (Fig. 4b, e). The comparison of this depth-varying time series plot with an analogous time-series plot defined by median isotherm depths from the entire study area (Fig. 4c, f) indicates little qualitative difference between these contrasting descriptions of dive activity patterns. We were also able to specify dive depth distributions and time allocations from TAT with greater precision, for example by stating that on average $\geq a\%$ of species b time is spent between $z_{min,T1}$ and $z_{max,T2}$ depth (*i.e.*, maximum depth range) over a geographic region of interest.

TAT frequency histograms could alternatively have been interpreted directly based on the thermoregulatory demands and constraints imposed on the whales by ambient water temperatures. However, as homeothermic endotherms with efficient insulation

and counter-current heat exchange (Ryg *et al.* 2003), the depth distributions of odontocetes are likely more sensitive to variables such as the vertical distributions of preferred prey, the physiological limits of diving capacity (Noren and Williams 2000), and potentially neutral buoyancy thresholds (Miller *et al.* 2004*b*). The distributions of many mesopelagic and some bathypelagic prey are most directly influenced by variables such as particulate organic matter flux (Martin *et al.* 1987) and downwelling light intensity (Ohman *et al.* 1983), which both attenuate as functions of depth. Thus, interpreting TAT histograms as approximate depth distributions likely provides greater insight into the diving behavior and habitats of deep-diving odontocete cetaceans compared to interpreting this information directly in terms of time-at-temperature.

Recommendations for Future Use

Despite the limitations and complexities of interpretation outlined above, our approach of estimating isotherm depths to interpret the dive behavior information transmitted in TAT histograms succeeded in describing vertical habitat use patterns and approximate dive depth ranges that converged with direct dive depth measurements in our case study species. This study thus demonstrates that, even under complex oceanographic regimes, summarized temperature outputs from SPOT tags can serve as a useful complementary tool to augment more direct measurements of dive behavior from SPLASH telemetry tags, TDRs, and DTAGs. In particular, this approach will be valuable in recovering underutilized dive information from prior studies that employed SPOT telemetry technology with a primary focus on ranging and spatial habitat use patterns. Tag technology is in a constant state of evolution, and in particular the incorporation of lightweight, relatively inexpensive, and low power consumption pressure sensors has become standard in more recent models of satellite telemetry tags. While the choice of telemetry technology will always remain dependent on the specific questions addressed by each study, using less precise but still informative SPOT model tags may become harder to justify in future studies of protected species such as cetaceans, where from an ethical standpoint data quality takes precedence over the total number of tags deployed. However, there remain several advantages to using SPOT tags unrelated to their lower cost. In particular these tags can provide longer battery life relative to SPLASH tags, which can extend both duration and strength of transmission. SPOT tags are also smaller and lighter than SPLASH tags (49 g *vs.* 63 g), which leads to moderately better flight characteristics and placement precision when remotely projected from longer distances. Therefore, a range of tradeoffs must be weighed in choosing between tag models, and in cases where high resolution and longer term tracks of spatial movement represents the primary focus of the study, the TAT interpretation approach outlined here can allow some additional inference to be gleaned on diving. Furthermore given the cost difference between SPOT and SPLASH models at the time of this study (*i.e.*, SPOT were 61% of the cost of SPLASH in the LIMPET configuration), SPOT models may also be widely applicable in studies of nonprotected species such as highly migratory fishes (*e.g.*, scombrids and elasmobranchs) where the precision of dive behavior estimates is balanced by the large number of tag deployments necessary to recover information.

Oceanographic regimes and hydrographic sampling densities in potential study areas are also critically important considerations in assessing the applicability of the methods outlined in this study. This study benefitted from a nearly linear decline

from 23°C–28°C in the surface mixed layer to <4°C over the upper 1,200 m of the water column in our study area (Fig. 1a). This allowed temperature categories spaced at 2°C intervals (*i.e.*, 20× greater than the ±0.1°C reported accuracy of SPOT thermistor, Wildlife Computers 2013) to define relatively narrow (~70–200 m) depth intervals, providing sufficient resolution to differentiate the dive ranges exhibited by most of the deep-diving species in our case study (Fig. 5). The relative stability of thermal structure over a 24 yr period of hydrographic sampling (Fig. 1a) in our study area also enabled the use of a climatological mean (1990–2014) as a useful approximation of the depth of the temperature strata. To maximize the granularity of dive patterns that can be resolved, careful thought and planning must be applied in tailoring the SPOT temperature bins to the thermal regime in the study area of interest, as well as the behavioral questions of interest.

The results in this study also benefitted from the relatively high density of hydrographic sampling in our study, which enabled the characterization of climatological thermal structure at a fine spatial resolution. This fine scale characterization was necessary given the complex bathymetry and the dynamic flow regime within our study area. However, the interpolation methods applied in this study could also be effectively implemented in study areas with less dense and/or frequent hydrographic sampling, where the thermal structure varies less in space and time. Areas with relatively low spatiotemporal variation in thermal structure and sufficient temperature contrast between surface and deep waters occur primarily over large areas of the northern and southern hemisphere subtropical gyres away from boundary currents. Moreover, with the continuing expansion of the global Argo profiling float array since the early 2000s, spatial and temporal sampling of temperature within the interiors of oceans worldwide is rapidly expanding. Thus, these approaches may be applicable in many areas where research on cetaceans and other large oceanic predators is conducted using SPOT tags (*e.g.*, Hawaii, Azores, Canary Islands, Mediterranean Sea, and subtropical Australia).

Acknowledgments

We are grateful to Charlotte Dunn and Leigh Hickmott at the Bahamas Marine Mammal Research Organisation (BMMRO) for their contributions to field research and project planning. We would also like to thank Dean Roemmich, Cesar Rocha, and Nick Cavanaugh of Scripps Institution of Oceanography for their guidance in sourcing physical oceanographic data and implementing an Objective Analysis interpolation approach. We would like to thank Brice Semmens, Lynn Talley, and Paul Dayton for their valuable input on the manuscript. We also thank dedicated field biologists Robert Pitman, Olivia Patterson, Aaron Banks, Marie Guilpin, Kendria Ferguson, Eric Lewallen, and Edward Adderley for their contribution to field efforts. We made use of data collected and made freely available by the International Argo Program and the national programs that contribute to it (http://www.argo.ucsd.edu, http://argo.jcommops.org). Finally, we are also very grateful to the captains and crews of the R/V *Walton Smith* and M/V *Slumber Venture* for their outstanding support of our research efforts. Funding for tagging efforts in the Bahamas were supported by the U.S. Navy Office of Naval Research (grant N000140710120), NAVFAC (grants N002441110021, N002441210007 and contract N6660413P2671), and the Strategic Environmental Research and Development Program (award RC-2114). Tagging was conducted under Bahamas Marine Mammal Protection Permit #12A. Tag types, methods of deployment, and sample sizes were all reviewed and approved by BMMRO's Institutional Animal Care and Use Committee (IACUC).

Literature Cited

Aguilar de Soto, N., M. P. Johnson, P. T. Madsen, F. Díaz, I. Domínguez, A. Brito and P. Tyack. 2008. Cheetahs of the deep sea: Deep foraging sprints in short-finned pilot whales off Tenerife (Canary Islands). Journal of Animal Ecology 77:936–947.

Aitchison, J. 1986. The statistical analysis of compositional data. Monographs on Statistics and Applied Probability. Chapman & Hall Ltd., London, U.K.

Andrews, R. D., R. L. Pitman and L. T. Ballance. 2008. Satellite tracking reveals distinct movement patterns for Type B and Type C killer whales in the southern Ross Sea, Antarctica. Polar Biology 31:1461–1468.

Aoki, K., M. Amano, T. Kubodera, K. Mori, R. Okamoto and K. Sato. 2015. Visual and behavioral evidence indicates active hunting by sperm whales. Marine Ecology Progress Series 523:233–241.

Aoki, K., M. Sakai, P. J. Miller, F. Visser and K. Sato. 2013. Body contact and synchronous diving in long-finned pilot whales. Behavioural Processes 99:12–20.

Arranz, P., N. A. de Soto, P. T. Madsen, A. Brito, F. Bordes and M. P. Johnson. 2011. Following a foraging fish-finder: Diel habitat use of Blainville's beaked whales revealed by echolocation. PLOS ONE 6:e28353.

Baird, R. W., D. L. Webster, D. J. McSweeney, A. D. Ligon, G. S. Schorr and J. Barlow. 2006. Diving behaviour of Cuvier's (*Ziphius cavirostris*) and Blainville's (*Mesoplodon densirostris*) beaked whales in Hawai'i. Canadian Journal of Zoology 84:1120–1128.

Baird, R. W., D. L. Webster, G. S. Schorr, D. J. McSweeney and J. Barlow. 2008. Diel variation in beaked whale diving behavior. Marine Mammal Science 24:630–642.

Baird, R. W., G. S. Schorr, D. L. Webster, D. J. McSweeney, M. B. Hanson and R. D. Andrews. 2011. Movements of two satellite-tagged pygmy killer whales (*Feresa attenuata*) off the island of Hawai'i. Marine Mammal Science 27:E332–E337.

Balcomb, K. C., and D. Claridge. 2001. A mass stranding of cetaceans caused by naval sonar in the Bahamas. Bahamas Journal of Science 5:2–12.

Beal, L. M., J. M. Hummon, E. Williams, O. B. Brown, W. Baringer and E. J. Kearns. 2008. Five years of Florida Current structure and transport from the Royal Caribbean Cruise Ship *Explorer of the Seas*. Journal of Geophysical Research: Oceans (1978–2012) 113: C06001.

Chassignet, E. P., H. E. Hurlburt, O. M. Smedstad, *et al*. 2007. The HYCOM (hybrid coordinate ocean model) data assimilative system. Journal of Marine Systems 65:60–83.

Clarke, K. R. 1993. Non-parametric multivariate analyses of changes in community structure. Australian Journal of Ecology 18:117–143.

Cox, T., T. Ragen, A. Read, *et al*. 2006. Understanding the impacts of anthropogenic sound on beaked whales. Journal of Cetacean Research and Management 7:177–187.

D'Amico, A., R. C. Gisiner, D. R. Ketten, J. A. Hammock, C. Johnson, P. L. Tyack and J. Mead. 2009. Beaked whale strandings and naval exercises. Aquatic Mammals 35:452–472.

de Jong, P., and J. Penzer. 1998. Diagnosing shocks in time series. Journal of the American Statistical Association 93:796–806.

Durban, J., and R. Pitman. 2012. Antarctic killer whales make rapid, round-trip movements to subtropical waters: Evidence for physiological maintenance migrations? Biology Letters 8:274–277.

Ford, J. K., J. W. Durban, G. M. Ellis, J. R. Towers, J. F. Pilkington, L. G. Barrett-Lennard and R. D. Andrews. 2013. New insights into the northward migration route of gray whales between Vancouver Island, British Columbia, and southeastern Alaska. Marine Mammal Science 29:325–337.

Frantzis, A. 1998. Does acoustic testing strand whales? Nature 392:29.

Gillespie, D., C. Dunn, J. Gordon, D. Claridge, C. Embling and I. Boyd. 2009. Field recordings of Gervais' beaked whales *Mesoplodon europaeus* from the Bahamas. The Journal of the Acoustical Society of America 125:3428–3433.

Hamilton, P., J. C. Larsen, K. D. Leaman, T. N. Lee and E. Waddell. 2005. Transports through the Straits of Florida. Journal of Physical Oceanography 35:308–322.

Hazen, E. L., D. P. Nowacek, L. S. Laurent, P. N. Halpin and D. J. Moretti. 2011. The relationship among oceanography, prey fields, and beaked whale foraging habitat in the Tongue of the Ocean. PLOS ONE 6:e19269.

Hooker, S. K., and R. W. Baird. 1999. Deep–diving behaviour of the northern bottlenose whale, *Hyperoodon ampullatus* (Cetacea: Ziphiidae). Proceedings of the Royal Society of London, Series B: Biological Sciences 266:671–676.

Johns, W. E., L. M. Beal, M. O. Baringer, J. R. Molina, S. A. Cunningham, T. Kanzow and D. Rayner. 2008. Variability of shallow and deep western boundary currents off the Bahamas during 2004–05: Results from the 26 N RAPID-MOC array. Journal of Physical Oceanography 38:605–623.

Johnson, D. S. 2013. *crawl*: Fit continuous-time correlated random walk models to animal movement data. R package version 1.4-1. Available at http://CRAN.R-project.org/package=crawl.

Johnson, M. P., and P. L. Tyack. 2003. A digital acoustic recording tag for measuring the response of wild marine mammals to sound. IEEE Journal of Oceanic Engineering 28:3–12.

Johnson, D. S., J. M. London, M.-A. Lea and J. W. Durban. 2008. Continuous-time correlated random walk model for animal telemetry data. Ecology 89:1208–1215.

Johnson, M., N. A. De Soto and P. T. Madsen. 2009. Studying the behaviour and sensory ecology of marine mammals using acoustic recording tags: A review. Marine Ecology Progress Series 395:55–73.

Kanzow, T., S. Cunningham, W. Johns, *et al*. 2010. Seasonal variability of the Atlantic meridional overturning circulation at 26.5°N. Journal of Climate 23:5678–5698.

Laist, D. W., A. R. Knowlton, J. G. Mead, A. S. Collet and M. Podesta. 2001. Collisions between ships and whales. Marine Mammal Science 17:35–75.

Lavery, T. J., B. Roudnew, P. Gill, *et al*. 2010. Iron defecation by sperm whales stimulates carbon export in the Southern Ocean. Proceedings of the Royal Society of London, B: Biological Sciences 277:3527–3531.

Leaman, K. D., P. S. Vertes, L. P. Atkinson, T. N. Lee, P. Hamilton and E. Waddell. 1995. Transport, potential vorticity, and current/temperature structure across Northwest Providence and Santaren Channels and the Florida Current off Cay Sal Bank. Journal of Geophysical Research: Oceans (1978–2012) 100:8561–8569.

Lee, T. N., W. E. Johns, R. J. Zantopp and E. R. Fillenbaum. 1996. Moored observations of western boundary current variability and thermohaline circulation at 26.5° in the subtropical North Atlantic. Journal of Physical Oceanography 26:962–983.

Macleod, C. D., M. B. Santos and G. J. Pierce. 2003. Review of data on diets of beaked whales: Evidence of niche separation and geographic segregation. Journal of the Marine Biological Association of the United Kingdom 83:651–665.

Madsen, P., M. Wahlberg and B. Møhl. 2002. Male sperm whale (*Physeter macrocephalus*) acoustics in a high-latitude habitat: Implications for echolocation and communication. Behavioral Ecology and Sociobiology 53:31–41.

Martin, J. H., G. A. Knauer, D. M. Karl and W. W. Broenkow. 1987. VERTEX: Carbon cycling in the northeast Pacific. Deep Sea Research Part A. Oceanographic Research Papers 34:267–285.

McCarthy, E., D. Moretti, L. Thomas, *et al*. 2011. Changes in spatial and temporal distribution and vocal behavior of Blainville's beaked whales (*Mesoplodon densirostris*) during multiship exercises with mid-frequency sonar. Marine Mammal Science 27: E206–E226.

McIntosh, P. C. 1990. Oceanographic data interpolation: Objective analysis and splines. Journal of Geophysical Research: Oceans (1978–2012) 95:13529–13541.

Miller, P. J., M. P. Johnson and P. L. Tyack. 2004*a*. Sperm whale behaviour indicates the use of echolocation click buzzes 'creaks' in prey capture. Proceedings of the Royal Society of London, Series B: Biological Sciences 271:2239–2247.

Miller, P. J., M. P. Johnson, P. L. Tyack and E. A. Terray. 2004*b*. Swimming gaits, passive drag and buoyancy of diving sperm whales *Physeter macrocephalus*. Journal of Experimental Biology 207:1953–1967.

Moretti, D., L. Thomas, T. Marques, *et al*. 2014. A risk function for behavioral disruption of Blainville's beaked whales (*Mesoplodon densirostris*) from mid-frequency active sonar. PLOS ONE 9:e85064.

Noren, S. R., and T. M. Williams. 2000. Body size and skeletal muscle myoglobin of cetaceans: Adaptations for maximizing dive duration. Comparative Biochemistry and Physiology A: Molecular and Integrative Physiology 126:181–191.

Ohman, M. D., B. W. Frost and E. B. Cohen. 1983. Reverse diel vertical migration: An escape from invertebrate predators. Science 220:1404–1407.

Olson, D. B., F. A. Schott, R. J. Zantopp and K. D. Leaman. 1984. The mean circulation East of the Bahamas as determined from a recent measurement program and historical XBT data. Journal of Physical Oceanography 14:1470–1487.

Pirotta, E., R. Milor, N. Quick, *et al*. 2012. Vessel noise affects beaked whale behavior: Results of a dedicated acoustic response study. PLOS ONE 7:e42535.

Roemmich, D. 1983. Optimal estimation of hydrographic station data and derived fields. Journal of Physical Oceanography 13:1544–1549.

Roemmich, D., and J. Gilson. 2009. The 2004–2008 mean and annual cycle of temperature, salinity, and steric height in the global ocean from the Argo Program. Progress in Oceanography 82:81–100.

Ryg, M., C. Lydersen, L. Knutsen, A. Bjørge, T. Smith and N. Øritsland. 1993. Scaling of insulation in seals and whales. Journal of Zoology 230:193–206.

Schorr, G., R. Baird, M. Hanson, D. Webster, D. McSweeney and R. Andrews. 2010. Movement patterns of satellite tagged Blainville's beaked whales (*Mesoplodon densirostris*) off the island of Hawaii: Implications for a greater risk from anthropogenic impacts? Endangered Species Research 10:203–213.

Schorr, G. S., E. A. Falcone, D. J. Moretti and R. D. Andrews. 2014. First long-term behavioral records from Cuvier's beaked whales (*Ziphius cavirostris*) reveal record-breaking dives. PlOS ONE 9:e92633.

Smeed, D., G. McCarthy, S. Cunningham, *et al*. 2014. Observed decline of the Atlantic meridional overturning circulation 2004–2012. Ocean Science 10:29–38.

Teloni, V., J. P. Mark, M. J. Patrick and M. T. Peter. 2008. Shallow food for deep divers: Dynamic foraging behavior of male sperm whales in a high latitude habitat. Journal of Experimental Marine Biology and Ecology 354:119–131.

Thomson, R. E., and W. J. Emery. 2014. Data analysis methods in physical oceanography. 3rd edition. Elsevier Science, Waltham, MA.

Trossman, D. S., L. Thompson and S. L. Hautala. 2011. Application of thin-plate splines in two dimensions to oceanographic tracer data. Journal of Atmospheric and Oceanic Technology 28:1522–1538.

Tyack, P. L., M. Johnson, N. A. Soto, A. Sturlese and P. T. Madsen. 2006. Extreme diving of beaked whales. Journal of Experimental Biology 209:4238–4253.

Tyack, P. L., W. M. Zimmer, D. Moretti, *et al*. 2011. Beaked whales respond to simulated and actual navy sonar. PLOS ONE 6:e17009.

van den Boogaart, K. G., and R. Tolosana-Delgado. 2008. "compositions": A unified R package to analyze compositional data. Computers & Geosciences 34:320–338.

Venables, W. N., and B. D. Ripley. 2002. Modern applied statistics with S. 4th edition. Springer, New York, NY.

Wallace, J. R. 2012. *Imap*: Interactive mapping. R package version 1.32. Available at http://CRAN.R-project.org/package=Imap.

Wang, J., and C. N. Mooers. 1998. Three-dimensional perspectives of the Florida current: Transport, potential vorticity, and related dynamical properties. Dynamics of Atmospheres and Oceans 27:135–149.

Watwood, S. L., P. J. Miller, M. Johnson, P. T. Madsen and P. L. Tyack. 2006. Deep-diving foraging behaviour of sperm whales (*Physeter macrocephalus*). Journal of Animal Ecology 75:814–825.

Wildlife Computers. 2013. Wildlife Computers data analysis programs. Available at http://wildlifecomputers.com/downloads.aspx.

Wood, S. 2006. Generalized additive models: An introduction with R. Taylor & Francis Group LLC, Boca Raton, FL.

Received: 12 July 2015
Accepted: 24 January 2016